Physical model assessment of the energy confinement time scaling in stellarators

A. Dinklage 1), H. Maaßberg 1), R. Preuss 1), Yu. Turkin 1), H. Yamada 2), E.Ascasibar 3), C.D. Beidler 1), T. Funaba 2), J.H. Harris 4,5), A. Kus 1), S. Murakami 6), S. Okamura 2), F. Sano 6), U. Stroth 7), Y. Suzuki 2), J. Talmadge 8), V. Tribaldos 3), K.Y. Watanabe 2), A. Werner 1), A. Weller 1) , M. Yokoyama 2)

1)   Max-Planck-Institut für Plasmaphysik, EURATOM-Association, Greifswald, Germany
2)   National Institute for Fusion Science, Toki, Gifu 509-5292, Japan
3)   Laboratorio Nacional de Fusión, EURATOM-CIEMAT, 28040 Madrid, Spain
4)   Australian National University, Canberra, Australia
5)   Oak Ridge National Laboratory, Oak Ridge, USA
6)   Kyoto University, Kyoto, Japan
7)   Institut für Plasmaforschung, Universität Stuttgart, Germany
8)   University of Wisconsin, Madison, USA

e-mail contact of the main author: dinklage@ipp.mpg.de

Abstract. The International Stellarator Confinement Database (ISCDB) is a joint effort of the helical device community. It is publicly available at http://www.ipp.mpg.de/ISS and http://iscdb.nifs.ac.jp. The validity of physics models is investigated employing ISCDB data. Bayesian model comparison shows differences in the confinement scaling of data subgroups. Theory-based assessment of pure neoclassical transport regimes, however, indicates scalability which is supported by experimental results in specific W7-AS scenarios. Therefore, neoclassical simulations are employed for predictive purposes, accounting for effects due to power deposition, plasma profiles, and the ambipolar radial electric field. Neoclassical case studies for W7-X are presented as examples for the neoclassical predictions to be considered as an upper limit of plasma performance.

1. The International Stellarator Confinement Database

Stellarator/heliotron research aims at an alternative fusion reactor concept. For a conclusive physics basis a comprehensive exploration of the plasma performance in existing devices is required. With respect to magnetic configurations and operational regimes, varieties in stellarator operation were revealed in earlier studies [1,2]. Consequently, a permanent assessment of confinement in stellarators and its relevance for reactor scenarios are required. As part of this effort, the International Stellarator Confinement Database (ISCDB) was re-initiated in 2004 and the ISS95 [3] has been extended to roughly 3000 discharges from eight different devices. In a first step, a unified scaling law ISS04 [1] was derived from an ISCDB subset consisting of roughly 1700 data. ISS04 largely confirms ISS95, but reveals the impact of the magnetic configuration which is formally described by a confinement time enhancement factor.

In addition to the data for global scaling considerations, ISCDB documents also special discharge scenarios, single parameter scans in power, density and rotational transform and even scans of the magnetic configuration (by variation of the major radius) in LHD [2]. The latter scan is also a case of neoclassical optimization due to inward shift of the plasma [4]. A second example is a density scan close to highest densities leading to the HDH bifurcation in Wendelstein 7-AS [5]. For HDH discharges the density scaling exponent was found to agree with the ISS04 scaling, however with a larger configuration factor which diminishes in the case of detached divertor plasmas. Third, the confinement in H-modes in W7-AS with broad density profiles compared to narrow density profile high-performance discharges is an example of profile effects on τ_E which is not reflected by the confinement scalings. Finally,

high-electron-temperature electron-root discharges governed by the beneficial effect of the radial electric field [6, 7] indicate the role of local transport properties in stellarator plasmas.

The global confinement of nearly all discharges of the ISS04 database is dominated by anomalous transport. Only at fairly high temperatures does neoclassical transport become important due to its unfavorable temperature dependence in the long-mean-free-path $1/\nu$ - regime governed by ripple trapped particles. It is this small subset of discharges (mainly from W7-AS) which allows for the confirmation of neoclassical modeling for the confinement, and is an example for theory-based extrapolations for W7-X, and in a future step, to reactor scenarios.

This paper is devoted to an assessment of physical models with respect to scaling laws. The first part deals with physical model comparison for global confinement data employing Bayesian model comparison techniques. In the second part purely neoclassical τ_E scalings are derived. The study is completed by predictive scans of neoclassical simulations for Wendelstein 7-X discharges which are compared with ISS95.

2. Model comparison for global confinement data scaling

Scaling laws are used both as a reference and for extrapolation. The latter purpose requires a careful assessment of the validity of scaling laws. A powerful approach is the application of dimensional constraints due to Connor and Taylor [8], followed e.g. by Christiansen et al. [9]. The basic idea as applied in this paper is to test the compatibility of data with a physics model. Requiring the same invariance behavior of the basic equations determining confinement and the scaling relation under similarity transformations puts constraints on the scaling model. If the model is a power law, the constraints are restrictions in the exponents [8]. Our technique to identify the most valid model for experimental data given is Bayesian model comparison [10]. This technique automatically obeys Occam's Razor and thereby punishes models of higher complexity, i.e. it weights consistently the number of model parameters considered. However, a key for the application of Bayesian model comparison is reliable error estimates of all model parameters but as well as in the target quantity.
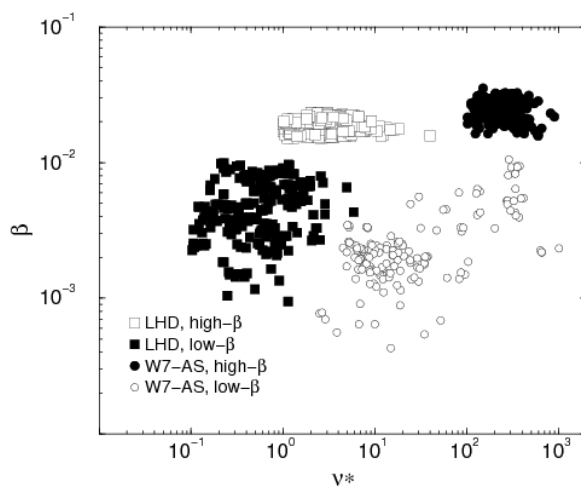

FIG. 1. β vs. collisionality of confinement data subsets from ISCDB. The low-beta data are full squares for LHD and open circles for W7-AS. The high-beta data are open squares for LHD and full circles for W7-AS.

An issue of particular reactor relevance is the beta scaling of global stellarator confinement. ISS04 indicates a small degradation of global stellarator confinement with the volume average plasma-β ($\tau_E \propto \beta^{-0.17}$). A caveat is due to the clustering of data in the beta-collisionality

space. Therefore, a detailed statistical analysis of the data subsets is necessary. In previous studies, early confinement data from W7-AS were identified to be consistent with a collisional low-β model [10]. The extension of ISCDB now allows us to test the model validity also for higher β data. FIG. 1 shows data from W7-AS and LHD widely spread in β and collisionality range. The data are separated into subgroups intuitively termed low- and high-β according to their relative appearance in FIG. 1 with respect to the β-axis.

According to the Connor/Taylor invariance principle [8] the scaling law ansatz is

$$(1) \qquad \tau_E \propto \sum_{k=1}^{E} B^{-1} \left(\frac{P}{na^4 B^3} \right)^{x_k-1} \left(\frac{a^3 B^4}{n} \right)^{y_k} \left(\frac{1}{na^2} \right)^{z_k} .$$

Note that this is actually an expansion into a series of single power laws. While the first term $(P/na^4 B^3)$ is contained in all CT-models, the occurrence of the $(a^3 B^4/n)$-term indicates that a model reflects collisional physics (otherwise the model is collisionless). Likewise, the $(1/na^2)$-term signifies high-β (otherwise low-β). Care has to be taken in the choice of the data in a sub group. For instance, $(a^3 B^4/n)$ is the decisive term in Eq. (1) to decide between collisionless and collisional CT-models. Since the minor effective radius a varies only marginally and it quite often happens that the machine conditions are such that the toroidal magnetic field B is the same for all discharges within a data set, there is no difference for this term and the 'collisional' term in Eq. (1), i.e. $(1/na^2)$. For such conditions, a model comparison for the above CT-models is not possible. Therefore, a wide spread of data must be ensured with respect to the terms in Eq. (1).
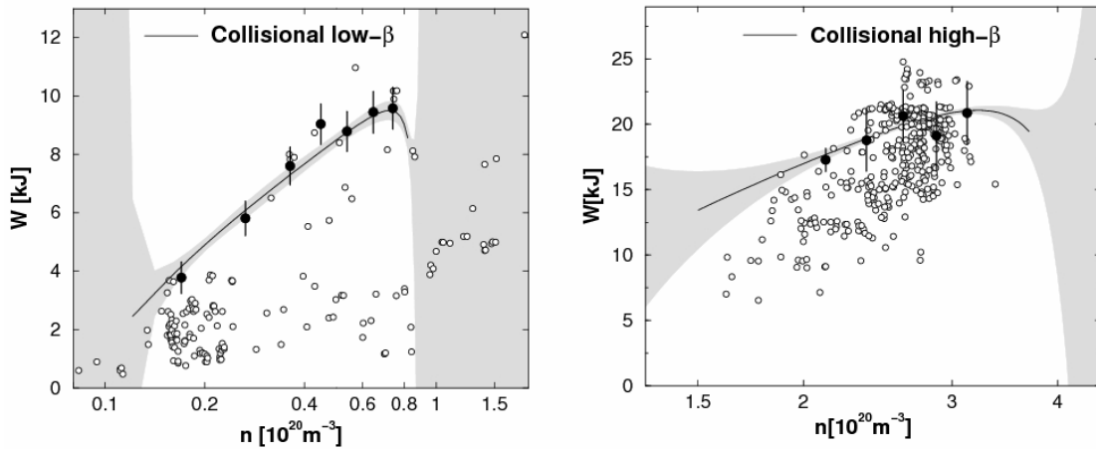

FIG. 2. Density scans for the low-β (left) and high-β (right) data set of W7-AS. The data from each set are shown in the open circles. Since they were measured for various settings of the other control parameters B,P and a, they are spread over the full W-range. Contrarily, the filled circles with error bars are average values of groups of data measured for a certain setting of the control parameters. Note that these values are not part of the data set used in the evaluation process. The result of the Bayesian estimation is shown by the solid line, where the grey shaded area is the confidence region.

The result of the model assessment is that the collisional low- and high-β models are most consistent with the low- and high-β data, respectively. Two additional tests for fluid models were unimportant in any set. However, note that the model probabilities are affected by the choice of the separation into low- and high-β subgroups, being somewhat arbitrary. With respect to collisionality the outcome must be more closely investigated: While the W7-AS high-β set is considered to be at the brink of the Pfirsch-Schlüter regime, the low-β data is in the $1/\nu$ regime of collisionality. Both were correctly identified with collisional CT-models.

The data basis for the subgroups of W7-AS is quite firm, so that deviations from a simple single power law behavior show up with high probability and an expansion order of $E=3$ in Eq. (1) is the most probable one, both for low- and high-β.

For the low-β data it was already revealed [8] that the most probable expansion with $E=3$ accounts for density saturation effects which cannot be described by a simple single-term power-law ansatz. This is demonstrated in FIG. 2 which depicts the variation of the density where the other control parameters B, P and a are set constant (low-β: B=2.53T, P=0.45MW and a=0.176m; high-β: B=1.18T, P=3.1MW and a=0.152m). Preliminary results for LHD show that the data basis is somewhat weaker and that collisional models win again for both subgroups, and $E=1$ for low-β and $E=2$ for high-β are already sufficient.

Testing physical models on confinement data indicate different transport mechanisms for different dimensionless parameters. A second result is the lack of predictability from simple power-law scalings. It is therefore questionable if global scaling laws derived for different discharge types and heating scenarios in different configurations and devices give a sufficient basis for performance predictions in reactor-relevant parameter regimes. The necessity to introduce a configuration-dependent confinement enhancement factor in ISS04 already emphasized this argument. In addition, one has to note that the present stellarator confinement database is mainly fed from small devices, i.e. the confinement is influenced by edge physics. In order to conclude on the reactor potential of stellarators, one has to confirm the basic physic mechanisms determining confinement; purely statistical approaches based on existing devices are less reliable.

3. Purely neoclassical energy confinement scaling

Neoclassical transport is by definition only local, and a representative radius, e.g. $r = 2/3\,a$, reflecting the global confinement is used for the analytical neoclassical τ_E scaling. In contrast, predictive neoclassical transport simulations as described in Sec. 4, leads to the estimation of the full radial profiles and, consequently, to the energy content and finally τ_E.

In the global neoclassical scaling approach, the total heat flux $Q_e + Q_i$ balances the deposited heating power P at the outer radius that is representative for the energy content (radiation losses are omitted in this discussion). At this radius, the analysis of the local neoclassical transport depending on n, T, B and ι leads to the τ_E scalings:

$$(2)\qquad P \approx Q_e + Q_i = -\sum_{\alpha=e,i} nT_\alpha \left[D_{21}^\alpha \left(\frac{n'}{n} - \frac{q_\alpha E_r}{T_\alpha} \right) + D_{22}^\alpha \frac{T_\alpha'}{T_\alpha} \right]$$

where D_{ij}^α is the neoclassical transport matrix, and E_r the ambipolar radial electric field. The D_{ij}^α depending on n, T, E_r, B and ι are formulated independently for the different collisionalities under the assumption of pure regimes, i.e. all particles of the same species α are in the same collisionality regime for all energies. Then, the normalized coefficients $\delta_{ij}^\alpha = D_{ij}^\alpha / D_{11}^\alpha$ are constants depending on the specific collisionality regime. Finally, a broad and flat density profile is assumed ($n' = 0$). With this assumption, $q_\alpha E_r / T_\alpha$ from the ambipolarity condition is linked to T_α' / T_α of the species dominating the particle flux at $E_r = 0$.

The first scenario reviews the Lackner-Gottardi scaling [13], i.e. the ion plateau scaling which holds for $Q_i \gg Q_e$ with ions being in the plateau regime $P \approx Q_i \propto nT_i D_{11}^i \left(\delta_{22}^i - \delta_{12}^i \delta_{21}^i \right) T_i'/T_i$, where $q_i E_r/T_i = \delta_{12}^i T_i'/T_i$. With $D_{11}^i \propto T_i^{3/2} B^{-2} t^{-1}$ one arrives at the ion-plateau scaling:

(3) $\tau_E \propto \dfrac{nT_i}{P} \propto n^{3/5} P^{-3/5} B^{4/5} t^{2/5}$

which is very close to the empirical ISS04 scaling, $\tau_E \approx n^{0.54} P^{-0.61} B^{0.84} t^{0.41}$.

The second scenario describes low-density ECRH discharges with $T_e \gg T_i$ resulting in $Q_e \gg Q_i$. Then, E_r is roughly proportional to T_e' (*electron root*) or negligible for Q_e (*ion root*). At outer radii with predominant contribution, the energy content (the small central *electron root* region is of minor importance) is determined by the $1/\nu$ transport with $D_{11}^e \propto T_e^{7/2} n^{-1} B^{-2}$ leading to $P \propto T_i^{9/2} B^{-2}$. Solving for T_e and substituting into τ_E leads to

(4) $\tau_E \propto n P^{-7/9} B^{4/9}$

This τ_E scaling differs from ISS04 but can be confirmed in selecting density and power scans for W7-AS ECRH discharges included in the ISS04 database; see FIG. 3.
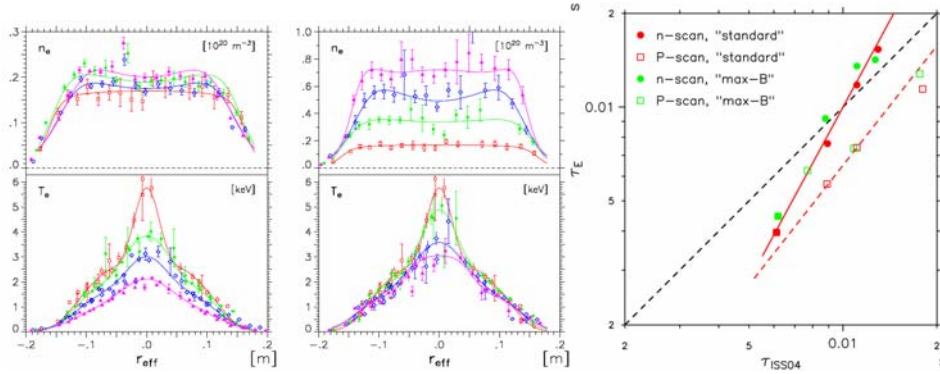

FIG. 3. Power (n_e, T_e profiles in the first column; P=0.2, 0.4, 0.8, 1.2 MW correspond to consecutively rising Te profiles) and density scan (n_e, T_e profiles in the second column, please note that the rise in temperature has a minor effect on τ_E) for CERC scenarios in $t = 1/3$ X2-ECRH discharges in W7-AS. The right subplot shows the energy confinement time vs. ISS04 and the neoclassical scaling according to Eq. (4) for these scans.

The third scenario is an example for which τ_E cannot be expressed in a simple power law as obtained by, e.g., linear regression analyses. Neoclassical τ_E scalings with $Q_i \approx Q_e$ must take the different dependencies of the electron and ion diffusion coefficients on n, T, B into account. Here $T_e \approx T_i \approx T$ is assumed for simplicity. As a long-mean-free-path example, the electrons are assume to be in the $1/\nu$-regime with $D_{11}^e \propto T^{7/2} n^{-1} B^{-2}$, and the ions in the $\sqrt{\nu}$-regime with $D_{11}^i \propto T^{-1/4} n^{1/2} B^{-1/2}$ where $q_i E_r/T = \delta_{12}^i T'/T$ is used to substitute the E_r dependence of D_{11}^i. Then, Eq. (2) takes the form $P = f(n, T, B)$ which cannot be solved analytically for T. Consequently, $\tau_E = \tau_E(n, P, B)$ cannot be formulated as a simple scaling law. The asymptotic limit $Q_e \gg Q_i$ is given by Eq. (4), whereas $Q_i \gg Q_e$ leads to

$\tau_E \propto n^{-1} P^{1/3} B^{2/3}$. But this asymptotic scaling is unrealistic since at higher densities (where $Q_i \gg Q_e$ is obtained) the assumption of the $\sqrt{\nu}$ regime for the ion diffusion coefficients fails and ion plateau scaling becomes dominant; see Eq. (3). The numerical solution at $Q_i \approx Q_e$ shows that the exponents of both the density and the power scaling approach the ISS04 exponents.

In W7-AS, "optimum confinement" discharges [14] with narrow density but fairly broad temperature profiles (quite different to H- or H*-mode discharges) are characterized by the agreement of both neoclassical Q_e and Q_i with the respective ones from power balance up to 2/3 of the plasma radius. In this sense, the main part of the energy content is determined by neoclassical transport with $Q_i \approx Q_e$. Although only the low-energy part of the electron and ion distribution functions correspond to the plateau regime, the agreement of τ_E with ISS04 is rather good. The dominant role of neoclassical transport in these high-performance discharges motivates the neoclassical predictive transport simulations for W7-X.

4. τ_E simulations for W7-X

Neoclassical predictive transport simulations [15] for both pure ECRH and pure NBI scenarios for the W7-X *standard* configuration are performed, and the simulated τ_E are compared with the ISS95 scaling. In the simulations, the shape of the density profile was fixed with a rather conservative gradient region (about 10 cm). For the outer 10 to 15% of the plasma radius, an anomalous heat diffusivity both for electrons and ions scaling as n^{-1} was added to the neoclassical transport coefficients. The time-dependent diffusion equations for the electron and ion temperatures (power balance) as well as for the radial electric field [16] are solved self-consistently up to steady-state. For ECRH and NBI heating scenarios, density and power scans are performed and the resulting τ_E is analyzed for each scan independently.

The ECRH scans are simulated for the X2-mode heating (140 GHz at B=2.5T), with densities $0.2 \times 10^{20} m^{-3} \leq n \leq 1 \times 10^{20} m^{-3}$ and heating power of 2MW $\leq P \leq$ 10MW with a central power deposition profile approximated by a Gaussian with 10 cm half-width. The X2-mode power deposition is nearly constant for W7-X in the density regime under investigation.
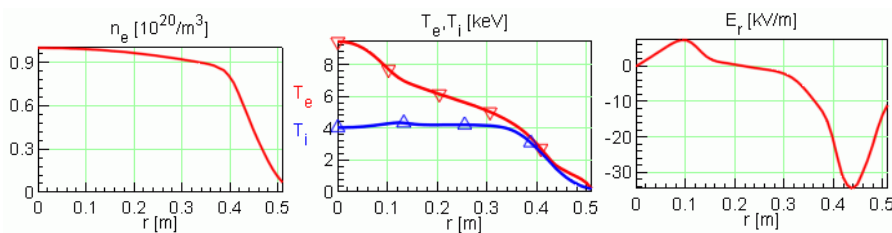

FIG. 4. Plasma profiles for a 10 MW ECRH predictive 1-D simulation of W7-X (density is given).

FIG. 4 shows a high-density example (cut off density at $1.2 \times 10^{20} m^{-3}$) at 10MW ECRH representing the full start-up ECRH power, resulting in a volume-averaged $\langle \beta \rangle \approx 3.8\%$. A marginal electron root with a small positive E_r is obtained within the central ECRH deposition zone with $T_e(r=0) \approx 10 keV$.

For NBI scenarios power deposition to ions and electrons is self-consistently calculated with the T_e and T_i profiles up to steady-state. In the NBI scans for 60 keV H+, also the injection at 1/2 and 1/3 of the full energy is taken into account leading to a fairly broad power-deposition profile. The density range is $0.5 \times 10^{20} m^{-3} \leq n \leq 3 \times 10^{20} m^{-3}$ where the lower limit is chosen to reduce shine-through losses below 20%. The power was varied within $2MW \leq P \leq 10MW$.
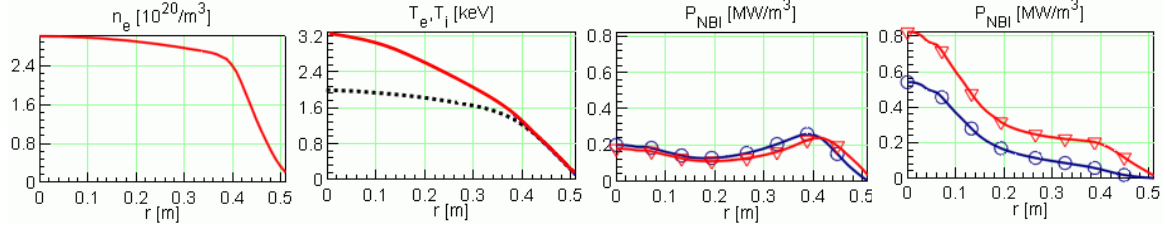

FIG. 5. Plasma profiles for a 10 MW NBI predictive 1-D simulation of W7-X (density is given). The dotted line in the temperature figure refers to p-NBI (power deposition shown in the third plot) and the solid line refers to n-NBI (power deposition in the fourth plot).

FIG. 5 shows the high-density, high-power example for positive NBI (p-NBI, 60 keV H$^+$) and for negative NBI (n-NBI, 150 keV H$^-$, full energy only). In the p-NBI case, the main power is absorbed at outer radii due to high densities at the edge. This leads to a τ_E degradation with density, whereas for the n-NBI case much higher central deposition allows for higher temperatures and improved global confinement. For example, $\tau_E = 0.45s$ and $\langle \beta \rangle = 4.2\%$ are obtained for p-NBI and $\tau_E = 0.60s$ and $\langle \beta \rangle = 5.4\%$ for n-NBI, respectively. These simulation results demonstrate that it is not the confinement that is degraded at high densities (see FIG. 2, right plot) but the NBI power deposition that is affected.

The density and power scans for both ECRH and NBI simulations are summarized in FIG. 6 where τ_E for W7-X simulations are added to experimental data from ISCDB. The significant improvement of the expected W7-X confinement with respect to ISS95 is consistent with the impact of the high W7-X elongation as described in the ITER ELMy H-mode scaling for tokamaks [17].
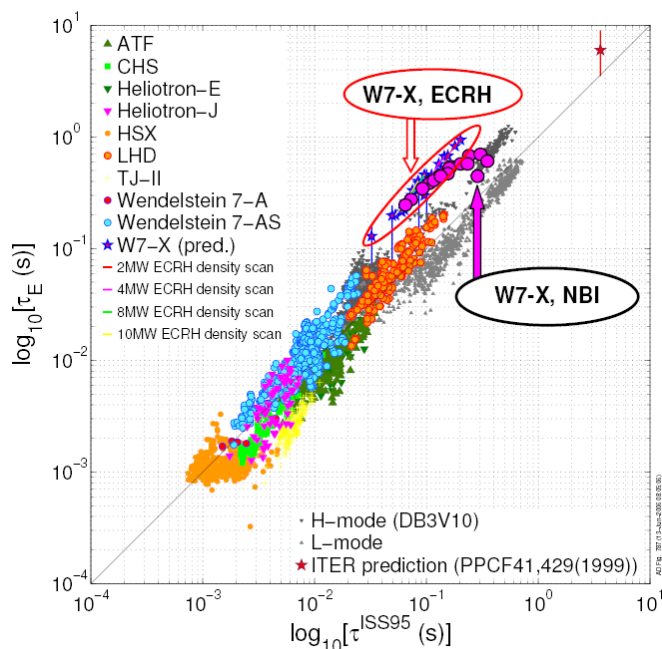

FIG. 6. Experimentally found energy confinement times and results from neoclassical simulations for W7-X versus ISS95. The W7-X simulations represent an upper limit of global confinement. The degradation of the τ_E for p-NBI is attributed to the outward shift of the power deposition with increasing density

5. Conclusions and Outlook

As empirically suggested in the previous ISS04 study, ISCDB shows different subgroups. This finding was quantitatively supported by Bayesian model comparison for different high-β data in LHD and W7-AS. The results of this paper indicate that low and high-beta data at different collisionalities are consistent with the respective scaling invariant physical model. This repeated confirmation applying Connor-Taylor invariance principles to generate physics models which can be tested, establishes a reliable method to obtain insight into the physical nature of data. This method is not restricted to the models presented in this analysis and might be extended to discharges dominated by anomalous transport, e.g. by testing the role of electromagnetic turbulence characterized by the magnetic Reynolds number.

Since the overall number of data is much smaller than in tokamaks, and the variety of configurations and operation modes is broader, the predictions must be supported by theory-based scalings. Limiting cases of neoclassical scaling are supported by some W7-AS discharges. More realistic predictions for W7-X are obtained by self-consistent 1D transport simulations.

The global 0D data base will be extended towards profile documentation of existing devices. LHD plays particular role here, allowing for validation of 1D transport models. Smaller existing devices like TJ-II, HSX and Heliotron-J complete the overall picture and may give further insight on the virtue of optimization and neoclassical mechanisms. Consequently, the 0D study ISCDB is the seedling, now maturing into the International Stellarator Profile Database ISPDB.

References

[1] H. YAMADA, J. HARRIS, A. DINKLAGE et al., Nucl. Fusion **45**, 1684 (2005)
[2] A. DINKLAGE, E. ASCASIBAR, C.D. BEIDLER, et al., Fusion Sci. Technol. – accepted
[3] U. STROTH, M. MURAKAMI, R.A. DORY et al., Nucl. Fusion **36**, 1063 (1996)
[4] S. MURAKAMI, A. WAKASA, H. MAASSBERG, et al., Nucl. Fusion **42**, L19 (2002)
[5] P. GRIGULL, K. MC CORMICK, Y. FENG, et al., J. Nucl. Mat. **313**, 1287 (2003)
[6] H. MAASSBERG, C.D. BEIDLER, U. GASPARINO et al., Phys. Plasmas **7**, 295 (2000)
[7] M. YOKOYAMA, H. MAAßBERG, C. BEIDLER et al. Fus. Sci. Technol. **50**, 327 (2006)
[8] J.W. CONNOR, J.B. TAYLOR, Nucl. Fusion **17**, 1047 (1977)
[9] J.P. CHRISTIANSEN, J.G. CORDEY, K.THOMSEN, et al, Nucl. Fusion **30**,1183 (1990)
[10] R. PREUSS, V. DOSE, W. VON DER LINDEN, Nucl. Fusion **39**, 849 (1999)
[11] A. WELLER, A.WERNER, J. GEIGER, et al, Plasma Phys. Contr. Fus. **45**, A285 (2003)
[12] J. NÜHRENBERG, R. ZILLE, Phys. Lett. A **114**, 129 (1986)
[13] K.LACKNER, N.A.O.GOTTARDI, Nucl. Fusion **30**, 767(1990)
[14] M. KICK, H.MAAßBERG, M.ANTON et al Plasma Phys. Contr. Fus. **41,** A549 (1999)
[15] YU. TURKIN, C.D. BEIDLER, A. DINKLAGE et al., 33th Conf. on Plasma Physics,
        Rome, Italy, June 19–23, 2006
[16] YU. TURKIN, H. MAASSBERG, C.D. BEIDLER et al, Fus. Sci. Tech. **50**, 387(2006)
[17] ITER Expert Groups, Nucl. Fusion **39**, 2175 (1999)